Design and control of an ultrasonic surface haptic device for longitudinal and transverse mode comparison

Diana Angelica Torres, Betty Lemaire-Semail, Christophe Giraud-Audine, Frédéric Giraud, Michel Amberg

Design and Control of an Ultrasonic Surface Haptic Device for Longitudinal and Transverse Mode Comparison

Diana Angelica Torres, Betty Lemaire-Semail, Christophe Giraud-Audine, Frederic Giraud, Michel Amberg*

**The authors are with Univ. Lille, Arts et Métiers Institute of Technology, Centrale Lille, Junia Hauts de-France, ULR 2697 - L2EP –, F-59000 Lille, France*

Abstract

The design and closed loop control of a device able to produce both longitudinal mode and transverse mode vibration, at about the same resonance frequency (60 kHz) are presented in this article. The structure uses an array of piezo-ceramics. A dynamic analysis is performed on the obtained modes, and their dynamic lumped parameters are identified. A closed loop control is performed to maintain the desired vibration amplitude in the presence of a finger. Longitudinal and transverse motion cartographies show that the objective of achieving and controlling pure modes independently has been achieved. Using this device, tribological, psychophysical and energetic analyses are carried out. The analyses show that in terms of friction measurements and perception, both modes produce equivalent results. In terms of active power losses, an advantage of the longitudinal mode over the transverse mode is observed due to the interaction with the finger

Keywords: Piezoelectric, Tactile Feedback, Longitudinal Vibrations, Transverse Vibrations, Control, Mathematical model, Resonance.

1. Introduction

Surface haptic devices for texture discrimination utilize techniques to achieve friction modulation, since differences in friction may create texture perceptions [1]. For doing so, ultrasonic vibration may be used. In this technique, a volume (resonator) is made to vibrate at ultrasonic frequencies, using piezoelectric actuators. As a consequence of this vibration, the friction of the surface is reduced, creating a sensation of ‘smoothness’ [1]. This phenomenon is usually referred to as “active lubrication”. The amount of friction reduction is dependent primarily on the speed of vibration (however, the mechanical properties of the probing object are also a determinant factor [2]–[5]). Achieving friction attenuation using vibrations in the low frequency ultrasound spectrum (LFU: from 20 to about 100 kHz) requires the vibration amplitude of the structure to achieve a few micrometers or more. In order to optimize the amount of actuators and energy necessary to achieve such displacement on a complete structure, the volume is generally excited at its resonance frequency.

There are several ways in which the material could be deformed, so different types of vibration are possible. In this work, we distinguish two types: The term "transverse vibration" is used to denote the deformation due to flexural strains, which produce an “out-of-plane” vibration. On the other hand, the term "longitudinal vibration" is used to denominate the deformation due to extension-compression strains, which produce an 'in-plane' vibration. The shape of the deformation (mode) is dictated by all the aforementioned parameters, plus the harmonic of the resonance frequency utilized.

Different ultrasonic surface haptic devices have been proposed and developed [6]–[9], and have progressively been included in the industry. With the design of a haptic knob [10], it was possible to observe that the presence of

* Diana Angelica Torres Guzman. Tel.: +33 (0)3-62-53-16-32.
E-mail address: diana.torres-guzman@univ-lille.fr

Click here to enter text.

the finger has an influence on the vibration of the plates. This influence may affect the perception of friction modulation from one user to another; for this reason, a closed-loop control of the vibration amplitude was introduced [11].

Even though the phenomenon of friction reduction with ultrasonic vibration has been thoroughly explored for several transverse modes, the effect and parametric dependence of the interaction mechanism through which friction is reduced with purely longitudinal vibration is seldom explored (with a few studies including [12]–[14]). However, longitudinal modes could potentially be used to improve or overcome certain challenges related to transverse modes, such as audible noise and plate integration in portable devices. It is also possible that longitudinal modes can be used in order to improve the energetic performance of surface devices.

It is therefore the objective of this article, to compare the two vibration modes in similar circumstances to determine the main advantages, possible drawbacks and design considerations for using longitudinal instead of transverse modes on surface haptic devices. To obtain this information a tribological, psychophysical and energetic comparison is presented. The energetic analysis is based on a preliminary active power study carried out in [15]. In order to get a comparative study of the performance of the longitudinal vs. transverse modes, it is necessary to conceive a device capable of producing both modes at a similar frequency.

The paper is organized as follows: The design and control of the two-mode ultrasonic surface haptic device are presented in section 2. Sections 3 to 5 deal with the tribology, psychophysical and energy comparison experiments and analyses. Finally, a discussion of the results and future research is presented in section 6.

2. 60 kHz Ultrasonic surface haptic device design and control

2.1. Pre-design and specifications

An ultrasonic surface haptic device was designed to evaluate the performance of longitudinal vibration compared to transverse vibration modes. In order to perform an accurate comparison of the two modes, we defined a set of design specifications. The first requirement for the device was to excite both modes independently at close vibration frequencies, without any mutual interference. Secondly, it was required that the motion source (electrical supply + actuators) of both modes be the same. Additionally, as a previous study [14] provided preliminary comparison results for vibration frequencies around 30 kHz, we decided to work at a higher frequency to extend the comparison range. The resonance frequency of 60 kHz was chosen, expecting an improvement in friction reduction performance of the devices [16]. Finally, the device was required to allow a clean flat exploration length of over 3 cm to allow tribological and psychophysical measurements. Finally, the wavelength of each mode was meant to allow a ‘uniform’ exploration along the desired surface. This means for the longitudinal mode, that half a wavelength should be larger than the exploration surface, and for the transverse mode that half a wavelength should be smaller than 1 cm, a dimension which allows a good homogeneity at the perceptual level [17].

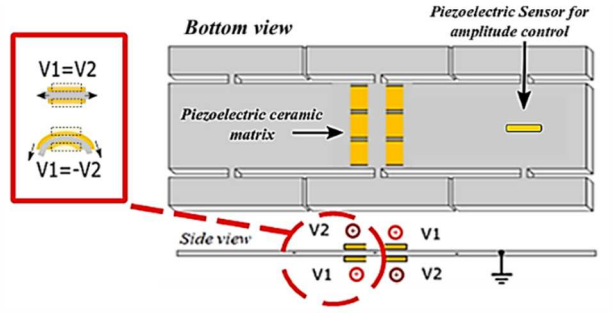

Figure 1. Bottom and side view of the plate design and setup to perform mode comparison on the same surface haptic device. The design includes 12 piezoelectric ceramics as source of motion and one as sensor for both modes.

The final designed structure is illustrated in Figure 1. The structure consists of an aluminum plate with a matrix of 12 piezoelectric ceramics (6 on each side) glued to the center of the device on the top and bottom sides, and a separate one glued on the bottom surface to serve as motion sensor. The resonator (aluminum plate) is attached to an immobile aluminum section through a series of isthmuses situated approximately at the vibrational nodes of both modes. A damp-proof polymeric sheet is glued to the aluminum beam on both sides of the actuator matrix on the top facet of the device.

To excite each mode selectively, the matrix of piezoelectric ceramics is placed and connected to follow the same basic principles as proposed in [11]; the deformation induced on the plate is the result of opposite surface tensions induced in both sides of the plate by the piezoelectric ceramics.

The 'top' and 'bottom' side actuators are connected to two independent voltage sources (V1 and V2 on Fig. 1), with the common ground connected to the conductive plate. The ceramics bend creating a surface stress on the aluminum plate. When V1=V2, an extension is produced simultaneously on both sides of the aluminum plate, leading to the longitudinal mode. When V1 = -V2, one surface is stretched, while the other compressed, 'bending' the material, thus producing the transverse mode.

The geometry and placement of the motor ceramics were designed to obtain a symmetrical deformation for both modes with respect to the center of the plate. Additionally, we sought to minimize the ceramics' interference with the plate's deformation. For the transverse modes, for example, this meant that the length of the ceramics should be shorter than half a waveform length of the mode. It was, however, not sought to optimize the coupling of the ceramic placement and the mode deformation, as it would be hard to comply for both modes at the same time. This consideration is relevant for the energy analysis performed in section 5.

A sensing ceramic was necessary to perform wave amplitude closed-loop control. The placement and geometry of the sensing ceramic were designed specifically to maximize the sensitivity to the deformation of both modes, with a single sensor, while minimizing the interference with the deformation of the mode, as recommended in [18]. In practical terms, this meant that the sensing ceramic was required to be 'small' and placed simultaneously along a maximum of vibration for the transverse mode and on a vibrational node for the longitudinal mode. Moreover, in order to avoid sensing errors due to crosstalk interference, it was recommended to place the sensing ceramic away from the actuators. Previous work [19] has shown that the finger impedance in the bulk can be modelled as a simple mechanical damper. Practically, this means that in the presence of a finger, the resonance frequency of the mode is shifted and the quality factor Q is decreased. Both effects imply an attenuation of the vibration amplitude, which motivates the use of an amplitude control loop, which is designed and implemented as explained in appendix 1. Regarding the mode shape, it is assumed that the finger does not impose a significant kinematic constraint and thus the mode shapes are preserved. In consequence, the closed loop control at the point of the sensing ceramic guarantees symmetric even mode shapes, with controlled vibration amplitudes over the whole volume.

2.2. Plate dimensioning

In order to follow the established specifications, we proposed an analytical approach to the plate's dimensioning, based on a simplified mechanical model of vibration in solid bodies. Thanks to this analysis we were able to find an expression for the resonance frequency of both modes in terms of the plate's dimensions. The dimensions which helped minimizing the difference between the resonance frequencies of the two modes were calculated. The final design was chosen in function of the wavelength of the modes which could be produced around 60 kHz. A finite element analysis was then performed on the resulting geometry, to verify and deduce the final design. Following the finite element simulation, the resulting prototype is implemented for testing. A laser cartography helped to determine whether the desired specifications were achieved. These different steps are described in the following sub-sections.

A. Euler-Bernoulli approximation

To find an analytical expression for the resonance frequency of each mode (longitudinal and transverse) in function of the plate's dimensions, we considered that it was possible to approximate the behavior of the proposed structure of the resonator (Figure 1), to that of a uniform solid beam. Given that we planned to work at about 60 kHz, it was possible to perform this analysis using the Euler-Bernoulli beam approximation [20], [21].

Following this model, on the x, y, z plane, we consider a parallelepipedic elastic body, continuous and isotropic, with dimensions L, b, h, for length, width and height, as shown in

Figure 2, with $L \gg b$ and $L \gg h$. This volume has a transverse surface $S = bh$. The mechanical properties of Young Modulus, quadratic momentum and volumetric density of the material section, are represented by E_e, I and ρ respectively. Under external forces, the beam changes shape. According to the Euler-Bernoulli theorem, the displacement field $\mathcal{U}$ can be expressed with the vector $\mathcal{U} = [\chi + (z - z_m)\psi \quad 0 \quad \psi]$. We define χ as the longitudinal displacement and ψ as the transversal displacement and z_m is the mid plane location. According to these assumptions, one can write the wave equations as (1) and (2) for longitudinal and transverse vibration, respectively.

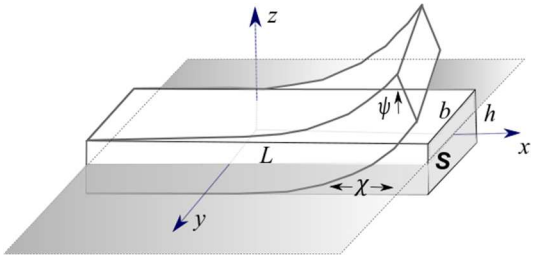

Figure 2. Euler-Bernoulli beam. χ and ψ are the out and in plane displacements with respect to the mid-plane z_m (in gray).

$$E_e S \frac{\partial^2 \chi}{\partial x^2} - \rho S \frac{\partial^2 \chi}{\partial t^2} = 0 \tag{1}$$

$$\rho S \frac{d^2 \psi}{dt^2} + E_e I \frac{\partial^4 \psi}{\partial x^4} = 0 \tag{2}$$

B. Resonance Frequencies

Under periodic excitation in a free-free regime, at certain frequencies, a sinusoidal stationary vibration is induced on the plate. In this case, equations (1) and (2) can be solved by a variable separation technique, which imposes relationship between the wave number β and the angular frequency ω.

In the case of longitudinal modes, the conditions for resonance to solve (1) can be written as $\frac{E_e}{\rho}{\beta_l}^2 = \omega^2$. The term β_l represents the wave number of the longitudinal mode. Free-free kinematic boundary conditions are assumed, which gives $\frac{\partial \chi(x)}{\partial x} = 0$ at the limits $x = 0$ and $x = L$. Applying these, we can find $\beta_l = k_L \pi / L$, with $k_L \in \mathbb{N}$. Each value of k_L defines one resonance frequency. With this result, it is possible to calculate the resonance frequency f_{rL} of the beam as in (3). The angular resonance frequency of the longitudinal mode is represented by ω_{rL}.

$$f_{rL} = \left(\frac{1}{2\pi}\right)\omega_{rL} = \left(\frac{1}{2\pi}\right)\frac{k_L \pi}{L}\sqrt{\frac{E_e}{\rho}} \tag{3}$$

Similarly, the resonance frequency of the transverse modes f_{rN} can be found by solving (2), using the free-free regime boundary conditions as explained in [20], [21] (moment $E_e I \frac{\partial^2 \psi}{\partial x^2} = 0$, and shear force $-E_e I \frac{\partial^3 \psi}{\partial x^3} = 0$). The solution is expressed in (4), with the wave number of each transverse mode k_N described by $\beta_n \approx (2k_N + 1)\frac{\pi}{2}$, given $k_N > 3$.

$$f_{rN} = \left(\frac{1}{2\pi}\right)\omega_{rN} = \left(\frac{1}{2\pi}\right)\left(\frac{\beta_n}{L}\right)^2 h\sqrt{\frac{E_e}{12\rho}} \quad (4)$$

In order to design a geometry which achieves 'close' frequencies $f_{rL} \approx f_{rN}$. Doing this we obtain (5) for $k_N > 3$. We cognize from the resulting equation that the dimensions which would provide similar transverse and longitudinal mode frequencies are independent from the material from which the device is made.

$$k_L \approx \frac{\pi h}{8\sqrt{3}L}(2k_N + 1)^2 \quad (5)$$

For this specific device, the 'height' dimension h was defined by the thickness of the available material, which in our case was 1.94 mm. The length of the plate L, and the harmonic numbers k_N and k_L were selected in consequence.

Given the geometry of the plate, and the desired exploration area, a mode $k_L = 3$ was selected for the longitudinal mode. It was expected that this deformation shape allowed placing one vibrational mode at each isthmus of the geometry. Then, the transverse mode k_N which produced the closest resonance without interference was deduced. At about 60 kHz, the plate length chosen was of about 128 mm, with $k_N = 14$. The selected dimensions of the resonator for simulation were therefore 128 mm x 30mm x 1.94mm, and the ceramics had a magnitude of 5 mm x 9mm x 0.3mm. These dimensions produced $f_{rL} = 57.4$kHz and $f_{rN} = 55.3$kHz according to (3) and (4), which we believed, was close enough to produce comparable results, while avoiding mutual interference.

A finite element simulation for the selected dimensions was performed around 60 kHz using Salome-Meca from Code_Aster [22]. The simulation included the geometry and material of the piezo-ceramics. The results are illustrated in Figure 3 (a). The modes obtained in the finite element simulation were measured at about 56.5 kHz for the longitudinal mode and 54.5 kHz for the transverse mode. Each mode could be excited and measured independently. The difference between the results from the simulation and the equations can be explained by the many differences between the device and the Euler-Bernoulli beam, such as the inclusion of the isthmus and immobile aluminum sections attached to the plate, plus the inclusion of the motor and sensing piezoelectric ceramics.

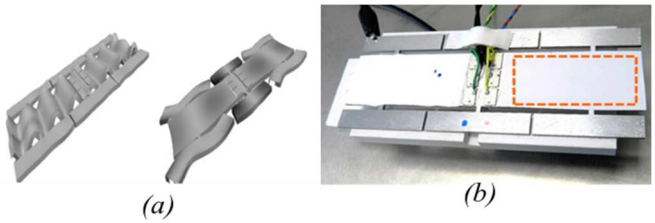

Figure 3. (a) Finite element simulation and (b) implementation of the device designed for the energetic comparison of transverse vs. longitudinal modes around 60 kHz. The device consists of an aluminum plate with 13 piezoelectric ceramics and a damp-proof polymeric cover glued to its surface. The framed section is the area which is cartographied in figure 4, and tested in sections 3, 4.

2.3. Cartography methodology and results

Figure 3 (b) illustrates the device implementation. Over it, an orange rectangle highlights a portion of one facet of the device. This framed 30 mm x 55 mm surface represents the area scanned for creating the cartography of both modes. From the simulation presented in Figure 3 (a), we cognize that both modes are symmetrical with respect to the center of the plate, so scanning the selected portion of the surface is sufficient to understand the behaviour of both facets of the structure.

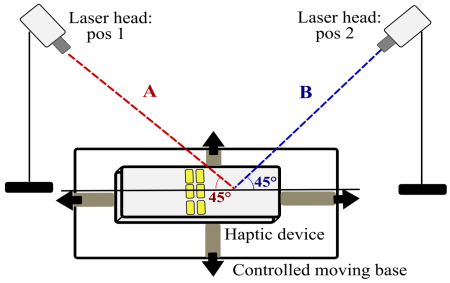

Figure 4. Setup for performing the cartography measurement of the longitudinal and the transverse modes.

The setup for measuring the longitudinal and the transverse motion is illustrated in Figure 4. The measurements were performed with the help of the Polytec OFV-5000 modular vibrometer base with Polytec OFV-505 sensor head. The ultrasonic surface haptic device was placed on a programmable moving base that located a selected matrix of points of the surface under the laser beam. Each point was measured twice, with the laser vibrometer placed at two different positions (+45° and -45° parallel to the *x* axis). The two beams reaching the measurement point (A and B in

Figure 4) produced two vibration amplitude measurements, noted w_A and w_B in (6) and (7), respectively. These raw data were used to deduce the magnitude of transverse w_N and longitudinal w_L displacement, by the difference and addition of each value, respectively, as described in (8) and (9).

$$w_A = w_N \sin(45°) + w_L \cos(45°) = \frac{\sqrt{2}}{2} w_N + \frac{\sqrt{2}}{2} w_L \quad (6)$$

$$w_B = w_N \sin(-45°) + w_L \cos(-45°) = \frac{-\sqrt{2}}{2} w_N + \frac{\sqrt{2}}{2} w_L \quad (7)$$

$$w_N = \frac{w_A - w_B}{\sqrt{2}} \quad (8)$$

$$w_L = \frac{w_A + w_B}{\sqrt{2}} \quad (9)$$

From the cartography results in Figure 5, we can observe that there are no parasitic modes around the resonance of the desired modes. We obtained, therefore, an almost pure longitudinal motion for the longitudinal mode (less than 5% of transverse motion), as well as an almost purely transverse motion for the transverse mode (less than 2% of longitudinal motion). This design allowed an exploration area through a length of over 3 cm between two nodes of the longitudinal mode.

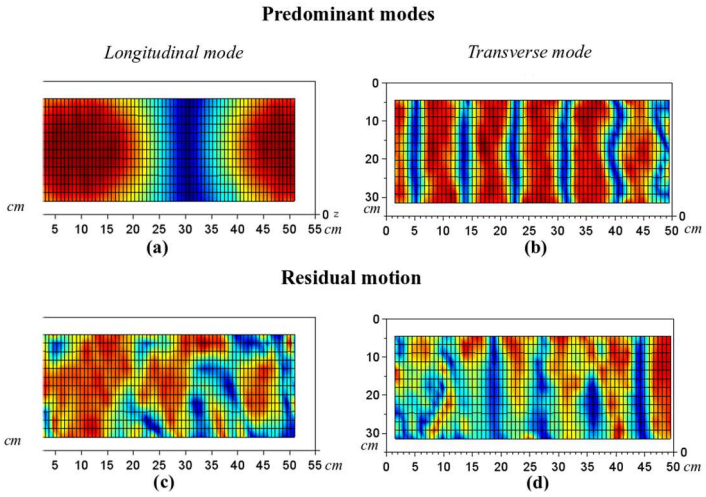

Figure 5. Cartography of one facet of the plate (framed in figure 3(b)) at resonance for transverse and longitudinal feeding conditions. (a) Longitudinal vibration amplitude at longitudinal mode conditions: 58 kHz, (V1=V2). Red corresponds to a maximum vibration amplitude of ~ 0.5 $\mu m_{p\text{-}p}$, dark blue 0 $\mu m_{p\text{-}p}$. (b) Transverse vibration amplitude at transverse mode feeding conditions: 56 kHz, (V1=-V2). Red corresponds to a maximum 0.1 $\mu m_{p\text{-}p}$, dark blue 0 $\mu m_{p\text{-}p}$. (c) Transverse vibration amplitude at longitudinal mode feeding conditions. Red corresponds to a maximum of 0.005 $\mu m_{p\text{-}p}$, dark blue to 0 $\mu m_{p\text{-}p}$. (d) Longitudinal vibration amplitude at transverse mode feeding conditions: Red corresponds to a maximum of 0.01 $\mu m_{p\text{-}p}$, dark blue 0 $\mu m_{p\text{-}p}$.

3. Tribology Comparison

To compare how effective a given mode is to produce a texture illusion, we need to analyze how much it is able to 'modulate' the friction of a surface for a given vibration amplitude. According to [23], the intensity of perception of a texture illusion is dependent on the amount of friction contrast $\frac{\Delta\mu}{\mu_0}$ felt during active exploration, with μ_0 being the friction of the finger against the surface without vibration, and $\Delta\mu = \mu_0 - \mu_{meas}$ the amount of variation of this friction achievable by a given vibration amplitude (μ_{meas} is the measurement of friction coefficient at a given vibration amplitude). In this section, we present a series of experiments, designed to produce the friction reduction comparison and analyze the main parameters influencing this effect in both modes.

3.1. Friction measurements

To perform the experimental tribological mode comparisons, a series of friction measurements were performed in three separate experiments. For these tests, we used the ultrasonic surface haptic device explained in section 2, including the closed loop amplitude control explained in the appendix. The implementation of the controller was achieved thanks to the use of a Digital Signal Processor (STM427 from ST Microelectronics). Two external power amplifiers (WMA-300 from Falco Systems) with outputs ranging up to 150 V_{p-p} were connected to provide V1 and V2.

In the first experiment, we performed the exploration velocity test. For this purpose, the ultrasonic surface haptic device was mounted on a tribometer, as depicted in Figure 6 (b). A series of measurements was then performed at two different exploration speeds (30 and 60mm/s). The tribometer probe performed several reciprocating motions over the surface along the *x* axis, while the device was made to vibrate at a constant amplitude. A series of vibration amplitude levels between 0 $\mu m_{p\text{-}p}$ and 1.6 $\mu m_{p\text{-}p}$ was tested and the mean measured friction coefficients were recorded. The pressing force was fixed at 0.5 N, and the plate vibration frequency at about 60 kHz.

The results for the relative friction coefficient ($\mu' = \mu_{meas}/\mu_0 = 1 - \Delta\mu/\mu_0$) measured for both modes, with the tribometer at different velocities are plotted in Figure 7(a). The measurements show a similar effect of the exploration velocity increase: as predicted by the models in [24] and [14], an increase in velocity reduces the performance of the devices in terms of friction reduction vs. vibration amplitude.

In the interest of comparing the performance of both modes at different resonant frequencies, an additional device was required. For this study, the results of the 60 kHz tribological measurements at 30 mm/s were compared to the measures recorded in [14] taken with the same tribometer probe at the same exploration velocity but with two devices. In this previous paper two ultrasonic surface haptic devices were used to compare transverse and longitudinal vibration at about 30 kHz. The results for μ' measurements at 30 kHz and 60 kHz are plotted in Figure 7(b). This result also confirms the model conclusions [16], [24] [15] that longitudinal and transverse modes perform better at higher frequencies, because the relative velocity of the vibration of the plate is very high compared to the probe velocity.

To test the effect of the probe mechanical impedance, the tribometer measurements that were taken with a hard probe were compared to a series of measurements taken during active exploration with a human finger, which was more deformable than the tribometer probe. A participant was requested to slide his/her finger over the ultrasonic surface haptic device surface along the x axis. In order to acquire the friction force measurements, the device was mounted on a three-axial force sensor (GSV-4USB from ME-Meßsysteme).

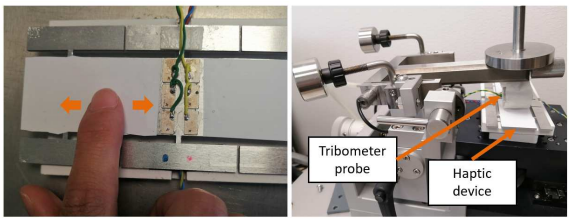

(a) **(b)**

Figure 6. Two methods used for friction measurements. (a) Top view of the active exploration of the surface: the participant performed several reciprocating motions at constant vibration amplitude, focusing on the exploration velocity and pressure, guided by visual aids. The friction measurements were performed by a three-axial force sensor attached to the base of the device. (b) Longitudinal view of the surface haptic device mounted on a tribometer, which performed and recorded the friction measurements. The tribometer's semi-spherical hard polymer probe was covered in plaster.

The participant was requested to attempt to maintain the same exploration speed, finger angle and pressure force during the measurements. To aid the participant, a visual interface has been programmed with the help of Opensesame graphic interphase software [25]. The visual interface guided the probing velocity and force with a moving arrow in the screen, the arrow indicated a motion of 30 mm/s and it turned green when the pressing force was within a defined threshold of +/- 0.1N around 0.5N.

The results for μ' are plotted in Figure 7 (c). As expected, the change in probe mechanical impedance produced a significant effect in the performance of the longitudinal as well as the transverse modes. The transverse mode performed significantly better with the finger than with the probe, and the longitudinal mode significantly better with the probe than with the finger. By these effects, it may be noted that at 60 kHz, with an exploration speed of 30mm/s, the longitudinal and transverse mode friction reduction vs amplitude results are very similar for both modes if we use a finger, especially at vibration amplitudes of over $1\mu m_{p-p}$ (some measurement error is added with human fingers due to many factors, including the difficulty to maintain the exploration speed, pressure force and angle).

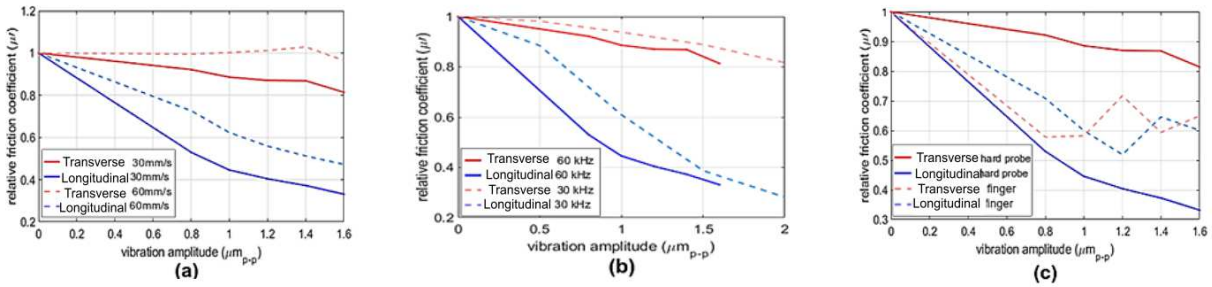

Figure 7. Tribology measurements of the relative friction coefficient at different vibration amplitudes for the two modes: Longitudinal (blue and light blue) and transverse (red and light red) (a) Exploration speed effect: in solid lines the measurements at 30 mm/s. In lighter dashed lines the measurements at 60 mm/s. (b) Frequency effect: In solid lines the measurements at 60 kHz. In lighter dashed lines, the measurements at 30 kHz. (c) Probe impedance effect: In solid lines the measurements with a stiff probe. In lighter dashed lines, the measurements with a finger.

4. Psychophysical Analysis

Thanks to a psychophysical analysis, it was possible to compare the perception intensity of friction contrast for both modes, for a set of vibration amplitudes, using the 60 kHz ultrasonic surface haptic device.

Data were collected from thirteen healthy volunteers aged between 18 and 50 (6 females). All participants gave written informed consent. The research conformed to the principles of the Declaration of Helsinki and experiments were performed in accordance with relevant guidelines and regulations.

To perform the tests, the setup in

Figure 8 was used. Before the tests, the participants were requested to clean and dry their hands. Then, they conducted a series of trials. In each trial, two textures (A and B) were presented. Each texture consisted of a closed loop ultrasonic vibration, modulated by a 10 Hz sinusoid that went from a value of 0 μm_{p-p} to a tested amplitude, as illustrated in Figure 8(c). One texture was generated with transverse vibration and the other with longitudinal vibration.

For each texture, the participants were asked to slide their finger over the surface of the ultrasonic surface haptic device along the x axis, focusing on the perceptual intensity the texture provided. They were then requested to

control their pressure force to be around 0.5N, and longitudinal speed close to 30 mm/s with the help of visual guides presented on the user's console. They were later told to decide which of the two textures produced a more 'intense' or clear sensation. The participants were able to feel both textures as many times as needed to make a choice, but they were not informed which texture corresponded to which mode.

It is important to note that the longitudinal mode did not provide a uniform sensation over a complete facet of the ultrasonic surface haptic device, since the nodes were too large and thus perceivable. For this reason, we reduced the exploration area to cover only the 2-3 cm closer to the piezoelectrics.

The amplitudes of the modulating signal were presented following a comparative one-up - one-down staircase test, such as the one explained in [26], where the reference was one fixed transverse mode modulating amplitude and the variable was the longitudinal mode modulating amplitude, which was meant to converge to the amplitude which produced an equivalent sensation in the transverse mode after a number of steps.

Each test was repeated for a series of reference transverse mode amplitudes ranging from 0.8 μm_{p-p} to 1.6 μm_{p-p}, with steps of 0.2 μm_{p-p} from one reference to the next. The tested levels were pseudo-randomized to prevent learning curve effects. Finally, a normality distribution test is performed on the obtained data to verify that a representative sample had been measured, such as in [26]. The results are presented as a boxplot in Figure 9. The line (X=Y) is presented for comparison.

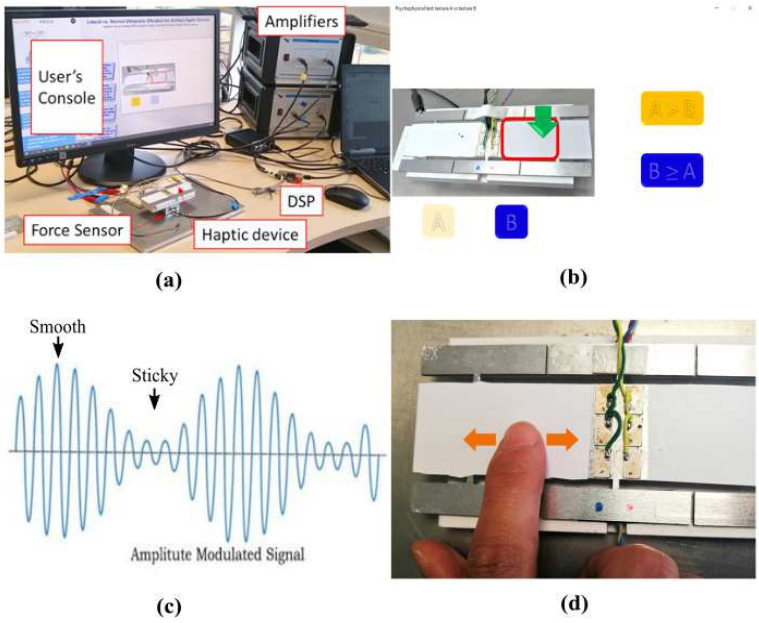

Figure 8. Setup for comparative psychophysical experiments. (a) Complete setup with all its parts. The user interacts only with the haptic device and the user's console. (b) View of the user's console with visual guides for force (arrow color) and velocity (arrow speed) of exploration. The user's console also allows the participant to change the mode (A or B) by clicking the corresponding virtual button and answer which is the mode that provides the strongest sensation, by clicking the virtual answer buttons (A > B or B ≥ A). The answers are used to perform a staircase type of comparative test. (c) Shape of the amplitude modulated vibration signal presented on the device. The amplitude of the envelope represents each tested vibration level, the frequency of the envelope is low to produce a texture. (d) View of the active exploration of the surface: the participant performs several reciprocating motions as the signal is presented, focusing on the intensity of the tactual feedback of the modulated vibration.

The results of this psychophysical test favor the longitudinal mode over the transverse mode at 60 kHz, especially at higher amplitudes (when the same comparison was performed at 30 kHz [14], it was concluded that transverse modes were the most performant of both modes). It is, however, possible to appreciate that the variance of the measurements at one reference is sometimes larger than the reference step.

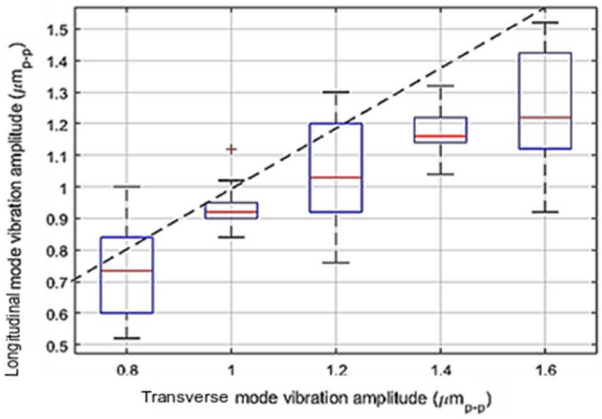

Figure 9. Box plot of the psychophysical test results of the comparison between transverse and longitudinal modes at about 60 kHz resonance frequency with a finger with exploration velocities around 30 mm/s. The boxes represent the vibration amplitudes for longitudinal and transverse modes which produce, in average, the same sensation when presented modulated by a 10 Hz sinusoid.

5. Energy Analysis

Sections 3 and 4 focused on the comparison of the performance in terms of amplitude vs. relative friction coefficient and amplitude vs. perception of friction contrast for the two modes. In both comparisons, it has been observed that for a finger exploring an ultrasonic surface haptic device vibrating at 60 kHz, longitudinal and transverse modes show a more or less equivalent performance in terms of vibration amplitude, with a slight advantage of the longitudinal mode in the psychophysical tests. This does not necessarily mean that their performance is equivalent in terms of energy consumption. As explained in [15] the energetic performance could be a determinant factor in the mode choice for haptic devices. Indeed, if the ultrasonic surface haptic device is to be used with a battery, for example, a better energetic performance may help increasing autonomy or reducing battery capacity specifications.

5.1. Energy losses in an ultrasonic surface haptic device

The energy consumption in an ultrasonic surface haptic device can be explained by two separate mechanisms: mechanical power losses and electric power losses [27]–[29]. The mechanical power losses are produced when the acoustic energy of the ultrasonic surface haptic device (including the resonator, the piezo ceramics and the glue) is dissipated due to internal material interactions, interactions with external forces and the surrounding environment. The electrical power losses, on the other hand, come from the hysteresis losses in dielectric and the hysteresis cycle in the piezoelectric coupling (hereby referred to as 'piezoelectric' losses) [27], [28], [30].

It is mostly agreed [27], [29]–[32] that the losses on the dielectric are negligible with regards to the mechanical and piezoelectric power losses in this type of ultrasonic surface haptic device. This is partly because we are working with hard ceramics, where dielectric losses are less significant [30]. Additionally, it can be observed that the proportion of material in the aluminum resonator is very large when compared to the amount of material in the piezoelectric actuators, rendering its associated dielectric losses less important in comparison.

The piezoelectric power losses, which may be significant, are related to the shape, mechanical and electrical properties and placement of the piezo-ceramics [29]. In [28], complex parameters are included in the dynamic equation of the piezo-ceramics to obtain an analytical model for the piezoelectric losses. However, in general, it can be assumed that for any given mode and plate shape, a geometry and placement of piezoelectric ceramics may be found, which maximizes the coupling with the mode [18], [33]. By doing this, the voltage requirements can be reduced, together with the piezoelectric losses. As explained in section 2.1, this type of optimization is hard to comply for both modes on the same device. For this reason, it was not carried out in the current study.

In [32] it is concluded that the chosen vibrational mode has an effect on the material's damping. In consequence, the minimization of the damping is a technique that has been used for energy optimization in previous studies. In [31], [32] for example, the thickness of the resonator is reduced in order to minimize the damping, thus optimizing the energetic consumption of the device. However, internal dissipation is not the only factor to consider in terms of energy optimization. Indeed, the interaction with external forces (produced by air and finger) could be determinant for improving the efficiency of the ultrasonic surface haptic device [32].

For the reasons exposed, this study focuses on highlighting the influence of the finger mechanical impedance on the losses for both modes. For doing this we performed two series of power measurements on the device. First, at no load, and then when there is a finger present.

5.2. Active power measurements at no load

To evaluate the active power requirements on the ultrasonic surface haptic device at no load, a series of measurements is made. In order to measure the active power consumption, a Fluke Norma 4000 power analyzer was connected to the motor ceramics. A frequency sweep was made at about +/-1 kHz around the resonance at three different voltage levels. The voltages were set for each mode to produce a vibration amplitude of around 0.8 $\mu m_{p\text{-}p}$, 0.6 $\mu m_{p\text{-}p}$ and 0.3 $\mu m_{p\text{-}p}$ at resonance.

The vibration amplitude was recorded together with the total active power measurements for each frequency. The measurements were performed three times at the same voltage levels at no load, and the mean of the three sweeps was recorded. The results for amplitude and active power measurements at no load condition around the resonance are presented in Figure 10.

The quality factor Q which is inversely proportional to the internal losses of the device, is affected by both dissipation and electric/mechanical energy storage elements. It may be observed from Figure 10 that Q is slightly higher for the transverse mode than for the longitudinal one. We can confirm similar results from the parameters identified in Table 1 (Appendix 1) With $Q_n = K_n/\omega_n D_n$, we obtain $Q_N = 216.9$, $Q_L = 206.4$.

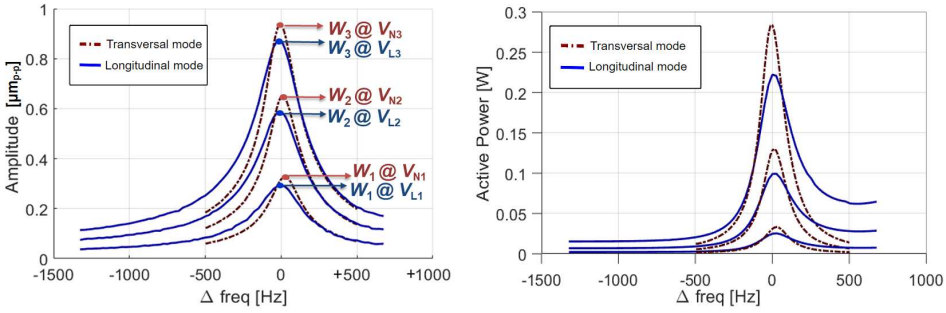

Figure 10. Vibration amplitude and active power measurements for transverse and longitudinal modes for three frequency sweeps at given voltages around the resonance of each mode. V_{Lk} and V_{Nk} represent the voltage needed to achieve vibration amplitudes W_k, with $k = 1,2,3$.

Additionally, the electromechanical conversion factor of the transverse mode $N_N = 0.3\ N/V$ is about 3.8 times higher than the one for the longitudinal mode $N_L = 0.0773\ N/V$, even though we used the same motor piezo-ceramics for both modes. This difference may be related to the positioning and size of the piezo-ceramics with regards to the obtained mode shapes. In this case, it appears that the positioning of the ceramics provides a better electromechanical coupling with the modal shape of the transverse mode. Consequently, the voltage needed to achieve a given vibration amplitude (in Figure 10, V_{Lk} and V_{Nk}) is over three times higher for the longitudinal mode than for the transverse mode ($V_{Lk} \approx 3V_{Nk}$ for $k = 1,2,3$). This voltage may perhaps produce additional conversion losses. However, if we observe the active power measurements, it can be concluded that, even though the longitudinal mode has a lower quality factor and requires higher voltages to reach a given vibration amplitude than the transverse mode, it also requires slightly less active power.

Overall, it can be observed that at no load, both modes show a similar energetic performance, with a slight advantage on the longitudinal mode, even though it requires higher voltage levels. The difference can be explained by the acoustic losses to the environment, which are higher for the transverse modes.

5.3. Impedance coupling: the effect of pressing with a finger

The measurements taken in 5.2 were repeated with a static finger pressing over a vibration maximum with a transverse force of 0.5N, and again with a finger pressing at 1N. The amplitudes and active power measurements were recorded over the three sweeps for each mode and plotted in Figure 11.

On the left, the figure shows the active power measurements at no load, compared to those with a finger on at two different pressure forces of 0.5N and 1N. On the right, the surfaces show the relationship between the vibration amplitude and the active power consumption over a range of frequencies around the resonance of each mode. A 'steeper' curve represents a worse performance than a flatter one.

Three results can be observed:

1- Attenuation: the amplitude is attenuated by over 54% by the presence of the finger with the transverse mode and only about 32% for the longitudinal mode (the measurements are performed in open loop).

2- Quality factor: the quality factor of the transverse mode is significantly reduced by the presence of the finger. An effect much less present in the longitudinal mode.

3- - Pressure force dependency: increasing the finger pressure from 0.5 to 1N has little to no effect on the frequency response of the longitudinal mode. However, the same pressure tends to shift the spectrum of the transverse modes towards lower frequencies.

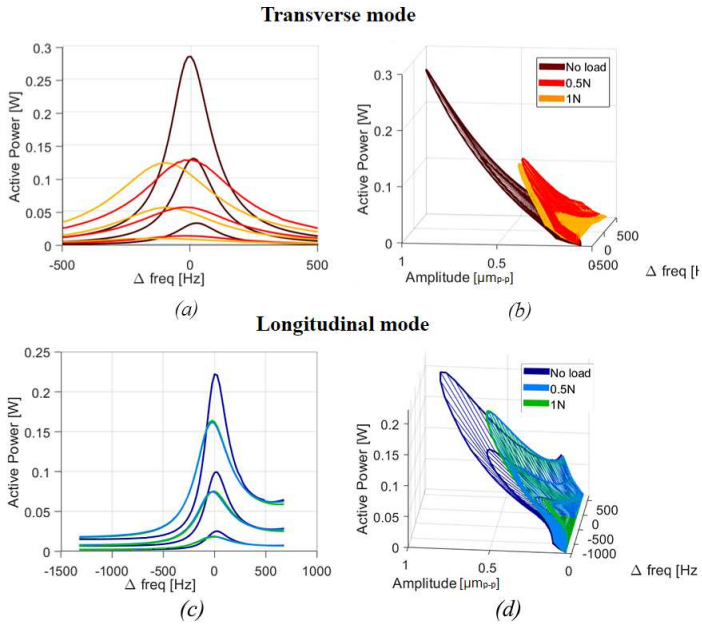

Figure 11. Active Power for a frequency sweep for transverse and longitudinal modes, for three constant voltage levels. The images present the measurements at no load vs. the measurements with a finger pressing the surface of the ultrasonic surface haptic device at constant pressures of 0.5N and 1N. Figures (a) and (c) represent active power vs. frequency shift. Figures (b) and (d) represent the surface formed by the measurements of active power vs. vibration amplitude around the resonance of each mode.

5.4. Amplitude vs. active power function

A final set of measurements was taken, which served to characterize the relationship between active power and vibration amplitude for each mode, considering the cases where there is no load, and when a finger is pressing with different forces. For the case where the finger is present, new measurements were taken at higher amplitudes, and the active power measurements at the resonance were recorded. With these measurements, it was possible to create a second order polynomial interpolation which produced a power/amplitude function for each mode at the different loads.

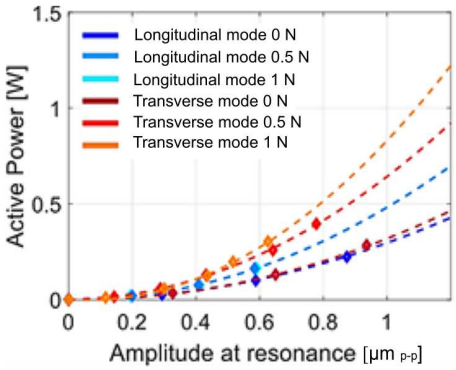

Figure 12. Active Power vs. Amplitude relation for the data measured at resonance. The quadratic fit of the longitudinal power measurements at loads of 0.5 N and 1 N are superposed

These relations are represented in Figure 12. In the figure, it can be observed that, while the consumption at no load is similar for both modes, the load presented by the finger increases significantly the value of the power function vs. amplitude for the transverse mode more than for the longitudinal mode. In other words, we may interpret that the finger acoustic impedance is smaller for the longitudinal mode. This effect will cause a higher wave attenuation with the transverse mode, and thus a better performance (less active power losses) with longitudinal mode.

This result helps confirming that the interaction mechanism with the finger is one of the decisive factors when considering energy performances of the ultrasonic surface haptic device.

6. Discussion

According to the analysis presented in sections 3-5, it may be possible to conclude that the use of longitudinal modes can prove to be advantageous for the creation of friction reduction ultrasonic surface haptic devices. However, there is a number of factors to take into consideration, which may require further research.

In terms of design, a series of challenges may be encountered when working with longitudinal mode devices. Firstly, the uniformity of the haptic feedback needs to be addressed. The fact that the wavelength of the longitudinal modes is significantly larger than that of the transverse modes in the low frequency ultrasonic spectrum up to 100 kHz, means that the surface velocity could not be uniform throughout the whole exploration area and there may be perceivable vibration nodes. This challenge is increased if we were to enlarge the desired width of the plate to work with a square, rather than a beam-like surface. Further research is therefore needed in order to establish how the design may allow a uniform sensation on a plane with longitudinal modes at frequencies around or higher than 60 kHz.

The use of higher frequencies derives from the result that the tribology and consequently the psychophysical performances are very dependent on the relative velocity of the wave against that of the finger. For this reason, longitudinal modes require higher frequencies to perform better than transverse modes. In the lower spectrum, the transverse mode tends to perform better as has been proven in [14] for 30kHz.

Extrapolating from the results obtained in numerals A and B of section 3.2, it is possible to conclude that irrespectively of the mode, the relative velocity of the probe against the vibration velocity of the plate is a key parameter for the friction attenuation due to ultrasonic vibration. The higher the vibration velocity is with respect to the finger, the better the results are. This confirms the results presented in [14], [24] using simplified first-order dynamic models. For this reason, it is recommended to increase this difference as much as possible. This can be achieved by working at higher resonant frequencies.

Finally, the direction of the exploration with regards to the wave propagation in longitudinal modes is a subject that needs a deeper assessment. Further research will therefore examine the interaction of the finger and the plate with longitudinal vibration at different exploration directions.

7. Conclusions

This article deals with the design and control of a surface haptic device based on ultrasonic vibration, aimed at comparing transverse and longitudinal modes. This ultrasonic surface haptic device consists of an aluminum plate with a set of 12 motor and 1 sensor piezoelectric ceramics glued to its surface. With this device, we are able to excite and control one longitudinal and one transverse mode independently at a frequency of about 60 kHz. Thanks to this, it is possible to analyze the comparison of the efficiency of both modes in terms of friction reduction, physical sensation and power losses at different vibration amplitudes.

In terms of friction reduction, a set of selected relevant parameters are analyzed. These are the resonance frequency of the mode, the velocity of exploration and the mechanic characteristics of the probing element. In the case of a finger exploring at mean exploration velocity of 30 – 60 mm/s over a surface vibrating around 60 kHz, both modes produce equivalent results, with a slight advantage for the transverse mode at low amplitudes (<1.4 μm_{p-p}).

The perception of friction contrast at different amplitudes was assessed with a group of participants thanks to a psychophysical staircase comparative test. The result show that at the tested conditions there exists a slight advantage for the longitudinal mode at higher vibration amplitudes (>1.4 μm_{p-p}).

Finally, the energetic assessment helped to conclude that the main factor affecting the active power losses on a surface haptic device dealt with the energy dissipation due to the presence of a finger. Because of the nature of the contact mechanics, the longitudinal acoustic impedance of the finger is smaller than the transverse acoustic impedance. For this reason, longitudinal modes have the potential to be more energy-efficient than transverse modes.

Future research in this subject will help improving the mechanical contact model between the finger and the plate with longitudinal modes at different exploration directions, and deal with the haptic feedback uniformity over a plate using longitudinal modes.

8. Acknowledgements

This work has been carried out within the framework of the Mint Project of IRCICA (CNRS Service and Research Unit 3380).

9. Appendix

9.1. Dynamic model of the plate at no-load condition for longitudinal and transverse modes

In order to control the vibration amplitude, it was necessary to model and identify the dynamic behavior and parameters of the ultrasonic surface haptic device. For the case of forced vibrations, we exploited the method of modal decomposition based on the orthogonality property of eigenmodes [34], [35].

Following this method, we can write the equation of a vibratory motion around a single non-dissipative vibration mode n as in (10) with M_n and K_n equal to the modal mass and stiffness specific to the mode. Hence, the force $F(t)$ required to obtain a given deformation $w_n(t)$ can be found as in (10).

$$F(t) = M_n \ddot{w}_n(t) + K_n w_n(t) \tag{10}$$

In reality, all systems lose energy, so a damping factor D_n is included in (10). Additionally, for considering the motion force from the piezoelectric transducer, $F(t)$ may be written as $N_n v$ (if we consider no additional external forces are acting on the device), with N_n representing the electro-mechanical transformation factor (which depends on the coupling of the ceramic and the vibration mode), and v the input voltage. This finally produces equation (11) [36].

$$N_n v(t) = M_n \ddot{w}_n(t) + D_n \dot{w}_n(t) + K_n w_n(t) \tag{11}$$

The variables w, $\dot{w}$ and $\ddot{w}$, represent the instantaneous displacement, speed and acceleration, respectively. The modal dynamic equation is valid for longitudinal χ as well as for transverse ψ displacements. Each mode, however is described by its own modal parameters.

Table 1. Parameters identified for the longitudinal and transverse modes [15]

Parameter	Mode	Symbol	Value
Electro-mechanical transformation factor	Longitudinal	$N_{L,3}$	0.0773 N/V
Modal Mass	Longitudinal	$M_{L,3}$	15.4 g
Modal Dampening	Longitudinal	$D_{L,3}$	27 N s/m
Modal Stiffness	Longitudinal	$K_{L,3}$	2017 N/m
Electro-mechanical transformation factor	Transverse	$N_{N,14}$	0.3 N/V
Modal Mass	Transverse	$M_{N,14}$	13.8 g
Modal Dampening	Transverse	$D_{N,14}$	22.1 N s/m
Modal Stiffness	Transverse	$K_{N,14}$	1678 N/m

The parameters of the implemented device were identified experimentally, as described in [11], [37]. The results are shown in Table 1. The sub-indexes $n = L, k_L$ and $n = N, k_N$ mean that the identified parameters correspond to either the longitudinal or the transverse mode, respectively, for the chosen harmonic number of each mode.

9.2. . Amplitude control in the rotating reference frame

One of the conclusions of [18] is that the vibration amplitude in both modes is attenuated by the presence of a human finger. This attenuation varies from one person to the other, due to the differences in their finger properties (e.g. humidity, rigidity, etc.). For this reason an experiment relating tactile response to vibration amplitude for a group of participants having different finger properties requires a closed loop amplitude control [37], [38].

In order to control a high frequency vibration both in amplitude and phase, [38] proposes a direct control in a virtual rotating reference frame, which can be performed by modulation/demodulation techniques. At steady state, the control follows references having slow dynamics, which can easily be handled by standard PI controllers. The actual voltages are then obtained by modulating their output. For doing this, we introduce the modulation process in the rotating reference frame, also called dq frame (d and q stand for 'direct' and 'quadrature'). It is the same process for both modes, even though the sign of V1 and V2, as well as the electromechanical lumped parameters (N, M, K and D) differ for each mode.

Assuming that $v(t)$ is a sinusoidal function, it can be represented by the use of complex phasors, as in (12)-(13), where $\underline{v}$ is the complex phasor of v, and $\underline{w}$ is the complex phasor of w. The real part of the phasor $\mathbb{R}\mathrm{e}(\underline{v}(t))$ is projected into the d axis and the imaginary part $\mathbb{I}\mathrm{m}(\underline{v}(t))$ on the q axis.

$$\underline{v}(t) = (V_d + jV_q)e^{j\omega t} \tag{12}$$

$$\underline{w}(t) = (W_d + jW_q)e^{j\omega t} \tag{13}$$

Replacing (12) and (13) in (11) , and writing N, M , D and K to represent N_n, M_n, D_n and K_n respectively, for any vibrational mode, leads to (14) and (15)

$$\mathrm{N}V_d = \mathrm{M}\ddot{W}_d + D\dot{W}_d + (K - M\omega^2)W_d - \omega(2M\dot{W}_q + DW_q) \quad (14)$$

$$\mathrm{N}V_q = \mathrm{M}\ddot{W}_q + D\dot{W}_q + (K - M\omega^2)W_q + \omega(2M\dot{W}_d + DW_d) \quad (15)$$

We assume that we operate the ultrasonic surface haptic device in such a way that the operating angular frequency ω is always close to the resonance of the mode, and the dynamic of the vibration is very fast compared to the evolution of the reference, or envelope. Because of this difference in dynamics, it is possible to assume that $|\ddot{W}_d| \ll \omega^2|W_d|$ and in the same way $|\ddot{W}_q| \ll \omega^2|W_q|$. Moreover, it can be assumed that $\frac{D}{K}|\dot{W}_d| \ll |W_d|$ and $\frac{D}{K}|\dot{W}_q| \ll |W_q|$. This way, we obtain (16) and (17) [36].

$$\mathrm{N}V_d = (K - M\omega^2)W_d - \omega(2M\dot{W}_q + DW_q) \quad (16)$$

$$\mathrm{N}V_q = (K - M\omega^2)W_q + \omega(2M\dot{W}_d + DW_d) \quad (17)$$

At the resonance, we may express $\omega \approx \omega_r = \sqrt{\frac{K}{M}}$. With this relation, it is possible to decouple the action of voltages V_d and V_q on each of the axes, thus obtaining the transfer functions (18) and (19) (a different approach is required if the ultrasonic surface haptic device is operated further from the resonance, and the coupling factor $(K - M\omega^2)$ becomes significant).

$$W_d = \left(\frac{1}{\omega}\right)\frac{{NV_q}/{D}}{{2M}/{D}\ s + 1} \quad (18)$$

$$W_q = \left(\frac{-1}{\omega}\right)\frac{{NV_d}/{D}}{{2M}/{D}\ s + 1} \quad (19)$$

The closed loop control structure was implemented for the obtained longitudinal and transverse modes using one PI controller for each axis. The design allows a response time $\tau = 1.1$ms for both modes, the dampening factor in closed loop is $\zeta = 1$, so there is no overshoot, and the steady state error is 0. In Figure 13 we present the step response for each mode at their resonance frequency in the *dq* reference frame. For simplicity, we chose a reference for W_{dref} equal to 0, and W_{qref} equal to $1.2\mu m_{p-p}$, so the amplitude measurement at no load depends mostly on voltage V_d (i.e. the amplitude is in quadrature with the phase of the voltage input) as can be deduced from equation (19).

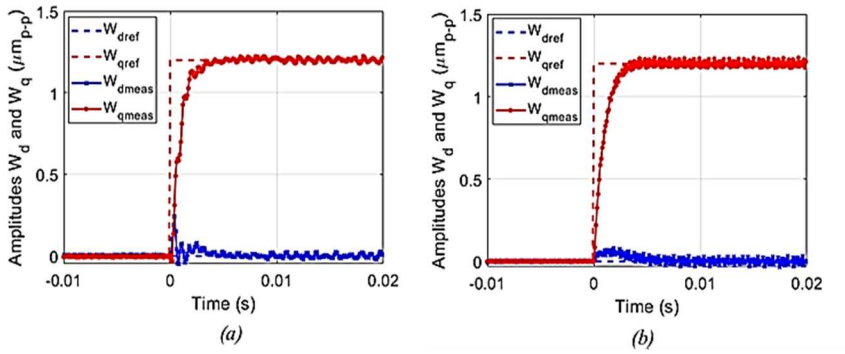

Figure 13. Measured values W_{dmeas} and W_{qmeas} step response for (a) transverse and (b) longitudinal modes around the resonance.

References

[1] Adams MJ, Johnson SA, Lefèvre P, Levesque V, Hayward V, Andre T, Thonnard J-L., "Finger pad friction and its role in grip and touch," *Journal of The Royal Society Interface*, vol. 10, no. 80, pp. 20120467–20120467, Dec. 2012, doi: 10.1098/rsif.2012.0467.

[2] R. F. Friesen, M. Wiertlewski, and J. E. Colgate, "The Role of Damping in Ultrasonic Friction Reduction," in *IEEE HAPTICS SYMPOSIUM 2016*, 2016, pp. 167–172. Accessed: Jan. 31, 2019. [Online]. Available: https://hal.archives-ouvertes.fr/hal-01454808

[3] J. Monnoyer, E. Diaz, C. Bourdin, and M. Wiertlewski, "Optimal skin impedance promotes perception of ultrasonic switches," in *2017 IEEE World Haptics Conference (WHC)*, Munich, Germany, Jun. 2017, pp. 130–135. doi: 10.1109/WHC.2017.7989889.

[4] J. Monnoyer, E. Diaz, C. Bourdin, and M. Wiertlewski, "Perception of Ultrasonic Switches Involves Large Discontinuity of the Mechanical Impedance," *IEEE Transactions on Haptics*, vol. 11, no. 4, pp. 579–589, Oct. 2018, doi: 10.1109/TOH.2018.2844186.

[5] M. Janko, M. Wiertlewski, and Y. Visell, "Contact geometry and mechanics predict friction forces during tactile surface exploration," *Scientific Reports*, vol. 8, no. 1, Dec. 2018, doi: 10.1038/s41598-018-23150-7.

[6] M. Amberg, F. Giraud, B. Semail, P. Olivo, G. Casiez, and N. Roussel, "STIMTAC: a tactile input device with programmable friction," in *Proceedings of the 24th annual ACM symposium adjunct on User interface software and technology - UIST '11 Adjunct*, Santa Barbara, California, USA, 2011, p. 7. doi: 10.1145/2046396.2046401.

[7] L. Winfield, J. Glassmire, J. E. Colgate, and M. Peshkin, "T-PaD: Tactile Pattern Display through Variable Friction Reduction," in *Second Joint EuroHaptics Conference and Symposium on Haptic Interfaces for Virtual Environment and Teleoperator Systems (WHC'07)*, Tsukuba, Japan, Mar. 2007, pp. 421–426. doi: 10.1109/WHC.2007.105.

[8] M. Wiertlewski, D. Leonardis, D. J. Meyer, M. A. Peshkin, and J. E. Colgate, "A High-Fidelity Surface-Haptic Device for Texture Rendering on Bare Finger," in *Haptics: Neuroscience, Devices, Modeling, and Applications*, vol. 8619, M. Auvray and C. Duriez, Eds. Berlin, Heidelberg: Springer Berlin Heidelberg, 2014, pp. 241–248. doi: 10.1007/978-3-662-44196-1_30.

[9] C. Winter, Y. Civet, and Y. Perriard, "Optimal design of a squeeze film actuator for friction feedback," *Proceedings of the 2013 IEEE International Electric Machines and Drives Conference (IEMDC 2013)*, 2013. https://infoscience.epfl.ch/record/191333 (accessed Aug. 07, 2019).

[10] F. Giraud, M. Amberg, and B. Lemaire-Semail, "Design and control of a haptic knob," *Sensors and Actuators A: Physical*, vol. 196, pp. 78–85, Jul. 2013, doi: 10.1016/j.sna.2013.03.012.

[11] S. Ghenna, F. Giraud, C. Giraud-Audine, M. Amberg, and B. Lemaire-Semail, "Modelling, identification and control of a Langevin transducer," in *2015 IEEE International Workshop of Electronics, Control, Measurement, Signals and their Application to Mechatronics (ECMSM)*, Liberec, Czech Republic, Jun. 2015, pp. 1–6. doi: 10.1109/ECMSM.2015.7208676.

[12] H. Xu, M. A. Peshkin, and J. E. Colgate, "UltraShiver: Lateral force feedback on a bare fingertip via ultrasonic oscillation and electroadhesion," in *2018 IEEE Haptics Symposium (HAPTICS)*, Mar. 2018, pp. 198–203. doi: 10.1109/HAPTICS.2018.8357176.

[13] E. Vezzoli, B. Dzidek, T. Sednaoui, F. Giraud, M. Adams, and B. Lemaire-Semail, "Role of fingerprint mechanics and non-Coulombic friction in ultrasonic devices," in *2015 IEEE World Haptics Conference (WHC)*, Evanston, IL, Jun. 2015, pp. 43–48. doi: 10.1109/WHC.2015.7177689.

[14] D. A. Torres Guzman, B. Lemaire-Semail, A. Kaci, F. Giraud, and M. Amberg, "Comparison Between Normal and Lateral Vibration on Surface Haptic Devices," in *2019 IEEE World Haptics Conference (WHC)*, Tokyo, Japan, Jul. 2019, pp. 199–204. doi: 10.1109/WHC.2019.8816124.

[15] D. A. Torres Guzman, B. Lemaire-Semail, F. Giraud, C. Giraud-Audine, and M. Amberg, "Energy Analysis of Lateral vs. Normal Vibration Modes for Ultrasonic Surface Haptic Devices," in *Haptics: Science, Technology, Applications*, vol. 12272, I. Nisky, J. Hartcher-O'Brien, M. Wiertlewski, and J. Smeets, Eds. Cham: Springer International Publishing, 2020, pp. 416–424. doi: 10.1007/978-3-030-58147-3_46.

[16] T. Sednaoui, E. Vezzoli, B. Dzidek, B. Lemaire-Semail, C. Chappaz, and M. Adams, "Friction Reduction through Ultrasonic Vibration Part 2: Experimental Evaluation of Intermittent Contact and Squeeze Film Levitation," *IEEE Transactions on Haptics*, vol. 10, no. 2, pp. 208–216, Apr. 2017, doi:

10.1109/TOH.2017.2671376.
[17] F. Giraud, M. Amberg, B. Lemaire-Semail, and C. Giraud-Audine, “Using an ultrasonic transducer to produce tactile rendering on a touchscreen,” in *2014 Joint IEEE International Symposium on the Applications of Ferroelectric, International Workshop on Acoustic Transduction Materials and Devices & Workshop on Piezoresponse Force Microscopy*, State College, PA, USA, Aug. 2014, pp. 1–4. doi: 10.1109/ISAF.2014.6922972.
[18] M. Doelle, D. Mager, P. Ruther, and O. Paul, “Geometry optimization for planar piezoresistive stress sensors based on the pseudo-Hall effect,” *Sensors and Actuators A: Physical*, vol. 127, no. 2, pp. 261–269, Mar. 2006, doi: 10.1016/j.sna.2005.08.014.
[19] M. Wiertlewski and V. Hayward, “Mechanical behavior of the fingertip in the range of frequencies and displacements relevant to touch,” *Journal of Biomechanics*, vol. 45, no. 11, pp. 1869–1874, Jul. 2012, doi: 10.1016/j.jbiomech.2012.05.045.
[20] M. Géradin and D. Rixen, *Mechanical vibrations: theory and application to structural dynamics*, Third edition. Chichester, West Sussex, United Kingdom: Wiley, 2015.
[21] L. Meirovitch, *Fundamentals of vibrations*. Long Grove, Illinois: Waveland Press, 2010.
[22] *Code_Aster*. EDF R&D. [Online]. Available: http://www.code-aster.org
[23] W. B. Messaoud, M.-A. Bueno, and B. Lemaire-Semail, “Relation between human perceived friction and finger friction characteristics,” *Tribology International*, vol. 98, pp. 261–269, Jun. 2016, doi: 10.1016/j.triboint.2016.02.031.
[24] Eric Vezzoli, Zlatko Vidrih, Vincenzo Giamundo, Betty Lemaire-Semail, Frédéric Giraud, et al.,“Friction Reduction through Ultrasonic Vibration Part 1: Modelling Intermittent Contact,” *IEEE Transactions on Haptics (ToH)*, vol. 10, no. 2, pp. 196–207, 2017, doi: 10.1109/TOH.2017.2671432.
[25] S. Mathôt, D. Schreij, and J. Theeuwes, “OpenSesame: An open-source, graphical experiment builder for the social sciences,” *Behav Res*, vol. 44, no. 2, pp. 314–324, Jun. 2012, doi: 10.3758/s13428-011-0168-7.
[26] P. Garcia, F. Giraud, B. Lemaire-Semail, M. Rupin, and M. Amberg, “2MoTac: Simulation of Button Click by Superposition of Two Ultrasonic Plate Waves,” in *Haptics: Science, Technology, Applications*, vol. 12272, I. Nisky, J. Hartcher-O’Brien, M. Wiertlewski, and J. Smeets, Eds. Cham: Springer International Publishing, 2020, pp. 343–352. doi: 10.1007/978-3-030-58147-3_38.
[27] R. Holland, “Representation of Dielectric, Elastic, and Piezoelectric Losses by Complex Coefficients,” *IEEE Trans. Son. Ultrason.*, vol. 14, no. 1, pp. 18–20, Jan. 1967, doi: 10.1109/T-SU.1967.29405.
[28] K. Uchino and S. Hirose, “Loss mechanisms in piezoelectrics: how to measure different losses separately,” *IEEE Trans. Ultrason., Ferroelect., Freq. Contr.*, vol. 48, no. 1, pp. 307–321, Jan. 2001, doi: 10.1109/58.896144.
[29] Y. Yang, B. Lemaire-Semail, F. Giraud, M. Amberg, Y. Zhang, and C. Giraud-Audine, “Power analysis for the design of a large area ultrasonic tactile touch panel,” *Eur. Phys. J. Appl. Phys.*, vol. 72, no. 1, p. 11101, Oct. 2015, doi: 10.1051/epjap/2015150051.
[30] K. Uchino , Hirose, S., “Loss mechanisms and high power piezoelectrics,” *J Mater Sci*, vol. 41, no. 1, pp. 217–228, Jan. 2006, doi: 10.1007/s10853-005-7201-0.
[31] F. Giraud, M. Amberg, R. Vanbelleghem, and B. Lemaire-Semail, “Power Consumption Reduction of a Controlled Friction Tactile Plate,” in *Haptics: Generating and Perceiving Tangible Sensations*, vol. 6192, A. M. L. Kappers, J. B. F. van Erp, W. M. Bergmann Tiest, and F. C. T. van der Helm, Eds. Berlin, Heidelberg: Springer Berlin Heidelberg, 2010, pp. 44–49. doi: 10.1007/978-3-642-14075-4_7.
[32] M. Wiertlewski and J. E. Colgate, “Power Optimization of Ultrasonic Friction-Modulation Tactile Interfaces,” *IEEE Transactions on Haptics*, vol. 8, no. 1, pp. 43–53, Jan. 2015, doi: 10.1109/TOH.2014.2362518.
[33] P. Sergeant, F. Giraud, and B. Lemaire-Semail, “Geometrical optimization of an ultrasonic tactile plate for surface texture rendering,” p. 12.
[34] D. J. Inman, “Active Modal Control for Smart Structures.,” *JSTOR*, vol. 359, no. 1778, pp. 205–219, 2001.
[35] W. Heylen, S. Lammens, and P. Sas, *Modal analysis theory and testing*, 2. ed. Leuven: Katholieke Univ. Leuven, Departement Werktuigkunde, 2007.
[36] F. Giraud, C. Giraud-Audine, M. Amberg, and B. Lemaire-Semail, “Vector control method applied to a traveling wave in a finite beam,” *IEEE Trans. Ultrason., Ferroelect., Freq. Contr.*, vol. 61, no. 1, pp. 147–158, Jan. 2014, doi: 10.1109/TUFFC.2014.6689782.
[37] F. Giraud and C. Giraud-Audine, *Piezoelectric actuators: vector control method*, 1st edition. Cambridge, CA:

Elsevier, 2019.
[38] S. Ghenna, F. Giraud, C. Giraud-Audine, and M. Amberg, “Vector Control of Piezoelectric Transducers and Ultrasonic Actuators,” *IEEE Transactions on Industrial Electronics*, vol. 65, no. 6, pp. 4880–4888, Jun. 2018.

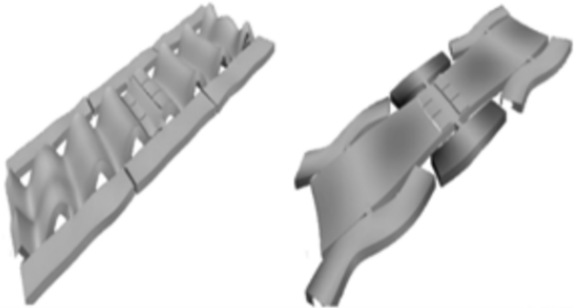

(a)

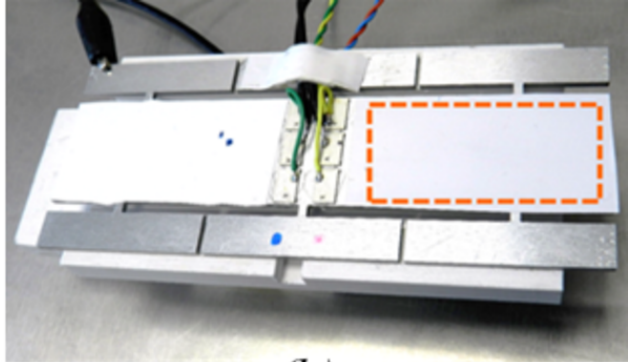

(b)